Two-Dimensional Superconductor with a Giant Rashba Effect: One-Atom-Layer Tl-Pb Compound on Si(111)

A. V. Matetskiy,[1,2] S. Ichinokura,[3] L. V. Bondarenko,[1,2] A. Y. Tupchaya,[1,2] D. V. Gruznev,[1,2] A. V. Zotov,[1,2,4] A. A. Saranin,[1,2,*] R. Hobara,[3] A. Takayama,[3] and S. Hasegawa[3]

[1]*Institute of Automation and Control Processes FEB RAS, 690041 Vladivostok, Russia*
[2]*School of Natural Sciences, Far Eastern Federal University, 690000 Vladivostok, Russia*
[3]*Department of Physics, University of Tokyo, Tokyo 113-0033, Japan*
[4]*Department of Electronics, Vladivostok State University of Economics and Service, 690600 Vladivostok, Russia*

(Received 28 April 2015; published 2 October 2015)

A one-atom-layer compound made of one monolayer of Tl and one-third monolayer of Pb on a Si(111) surface having $\sqrt{3} \times \sqrt{3}$ periodicity was found to exhibit a giant Rashba-type spin splitting of metallic surface-state bands together with two-dimensional superconducting transport properties. Temperature-dependent angle-resolved photoelectron spectroscopy revealed an enhanced electron-phonon coupling for one of the spin-split bands. *In situ* micro-four-point-probe conductivity measurements with and without magnetic field demonstrated that the (Tl, Pb)/Si(111) system transformed into the superconducting state at 2.25 K, followed by the Berezinskii-Kosterlitz-Thouless mechanism. The 2D Tl-Pb compound on Si(111) is believed to be the prototypical object for prospective studies of intriguing properties of the superconducting 2D system with lifted spin degeneracy, bearing in mind that its composition, atomic and electron band structures, and spin texture are already well established.

DOI: 10.1103/PhysRevLett.115.147003 PACS numbers: 74.78.Na, 74.25.fc, 74.25.Jb, 74.62.Bf

Metal-induced surface reconstructions on silicon (i.e., metal films having a monolayer and submonolayer thickness on silicon) have been intensively studied for more than 50 years, starting from the very early ages of modern surface science [1]. Because of an abundance of studies on the reconstructions having various structures and properties, it might be thought that most of the principal interesting phenomena in this field have already been elucidated and the main problems have been conclusively solved. However, seminal discoveries in the past five years have brought about two fascinating themes: giant Rashba effect and superconductivity in one-atom-layer metal films on silicon surfaces.

The Rashba effect [2,3], which resides in spin splitting of two-dimensional electronic states due to the spin-orbit interaction arising from space-inversion asymmetry, has been found to be especially pronounced ("giant") in Bi [4–6] and Tl [7–11] monolayers on a Si(111) surface. The only drawback of these systems is that their spin-split bands are nonmetallic, while for the spintronics applications one needs metallic spin-split bands to ensure considerable spin transport. However, it has recently been demonstrated that this shortage can be overcome by adding appropriate adsorbates to form 2D compound layers with metallic spin-split bands [12,13].

Two-dimensional superconductivity was discovered in In/Si(111) and Pb/Si(111) systems [14–22]. The most expressive results were obtained with double atom layers of In [23] and Pb [15] on Si(111), where superconducting transition temperatures T_c are as high as ~2.8–3.2 K [14,16,17,24] and ~3.65 K [15] for In and Pb double layers, respectively. However, one-atom-layer In and Pb on Si(111) also display superconducting properties, albeit at somewhat lower temperatures, $T_c \approx 2.4$ K for In [17] and $T_c \approx 1.1$–1.8 K for Pb [14,17].

In this Letter, we report on the discovery of a system that unites together the two themes mentioned above. We have found that alloying one monolayer of Tl with one-third monolayer of Pb (both ingredients being heavy metals with strong spin-orbit coupling and classical bulk superconductors) results in a one-atom-layer Tl-Pb compound on Si(111) that displays both Rashba-type spin splitting and 2D superconductivity. The occurrence of the spin-split metallic bands in the Tl-Pb layer on Si(111) has already been reported [12]. In the present study, we performed angle-resolved photoelectron spectroscopy (ARPES) measurements on the Tl-Pb compound as a function of temperature in order to evaluate the electron-phonon coupling (EPC) constant λ from the temperature dependence of surface-state energy widths. A large value of $\lambda \approx 1.6$ obtained for one of the spin-split metallic surface-state bands indicates an enhanced electron-phonon coupling, and hence provides a promise for observing superconductivity at a sizable temperature. Indeed, *in situ* micro-four-point-probe (MFPP) conductivity measurements showed the superconductivity transition at 2.25 K. The obtained transition temperature almost coincides with that for bulk Tl (2.38 K) and is considerably higher than that for one-atom-layer Pb on Si(111), ~1.1 K [17]. The superconducting transition was accompanied by Berezinskii-Kosterlitz-Thouless (BKT) transition as

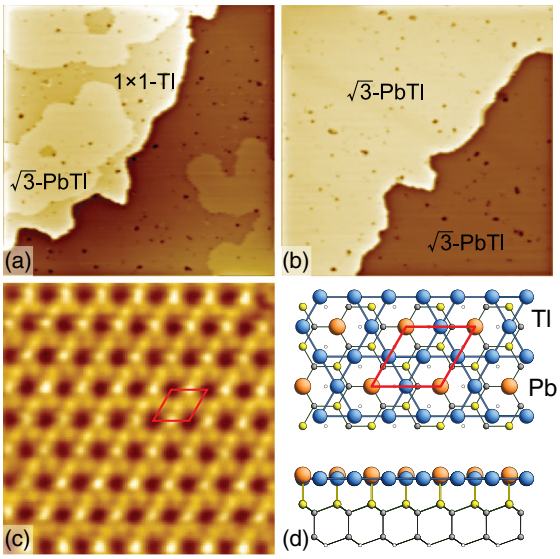

FIG. 1 (color online). Large-scale (150×150 nm^2) STM images showing formation of the Tl-Pb 2D compound on the Si(111)-(1 × 1)-Tl surface after RT deposition of (a) 0.18 ML Pb (intermediate stage) and (b) 0.33 ML Pb (final stage). Two atomic terraces are seen in each image. (c) High-resolution (5×5 nm^2) STM image of the (Tl, Pb)/Si(111) surface. (d) Atomic structure of the Tl-Pb compound. Tl atoms are shown by blue circles, Pb atoms by orange circles, top Si atoms by yellow circles, and deeper Si atoms by light gray circles. The $\sqrt{3} \times \sqrt{3}$ unit cell is outlined by a red frame.

revealed by current-voltage characteristics, indicating the 2D nature of the superconductivity.

Measurements were performed in the two separate UHV systems. STM and ARPES experiments were conducted in an Omicron MULTIPROBE system. STM images were acquired in a constant-current mode with a mechanically cut PtIr tip after annealing in vacuum. ARPES measurements were conducted using a VG Scienta R3000 electron analyzer and a high-flux He discharge lamp ($h\nu = 21.2$ eV) with a toroidal-grating monochromator as a light source. The *in situ* electronic transport measurements were performed with an UHV MFPP system in which the sample and the MFPP were cooled down to 0.8 K and a magnetic field up to 7 T was applied perpendicular to the surface. The apparatus was also equipped with RHEED for sample characterization with deposition [25].

Pristine $\mathrm{Tl/Si}(111) - (1 \times 1)$ reconstruction was prepared by depositing 1 ML Tl from a Ta-tube effusion cell onto a $\mathrm{Si}(111) - (7 \times 7)$ surface held at ~300 °C [1 ML $= 7.8 \times 10^{14}$ cm^{-2}]. Lead was deposited from a heated Pb-stuffed Mo-tube effusion cell onto the Tl/Si(111) surface held at room temperature. Starting from the onset of Pb deposition, the patches of the 2D Tl-Pb compound appear and grow in size with Pb dosing until they cover the entire surface at 1/3 ML Pb coverage [Figs. 1(a) and 1(b)]. In the STM images, the Tl-Pb compound differs from the parent Tl monolayer by brighter contrast and honeycomb-like appearance with $\sqrt{3} \times \sqrt{3}$ periodicity [Fig. 1(c)]. As determined in Ref. [12], the Tl-Pb compound layer is composed of honeycomb-chained trimers of Tl atoms with Pb atoms occupying the T_4 sites in the center of each honeycomb unit [Fig. 1(d)].

The most essential features in the (Tl, Pb)/Si(111) electron band structure are two metallic spin-split surface-state bands [denoted Σ_1 (Σ_1') and Σ_2 (Σ_2') in Fig. 2] [12]. In the Fermi-surface map, they appear as two split contours. For the Σ_1 (Σ_1') band, the outer contour

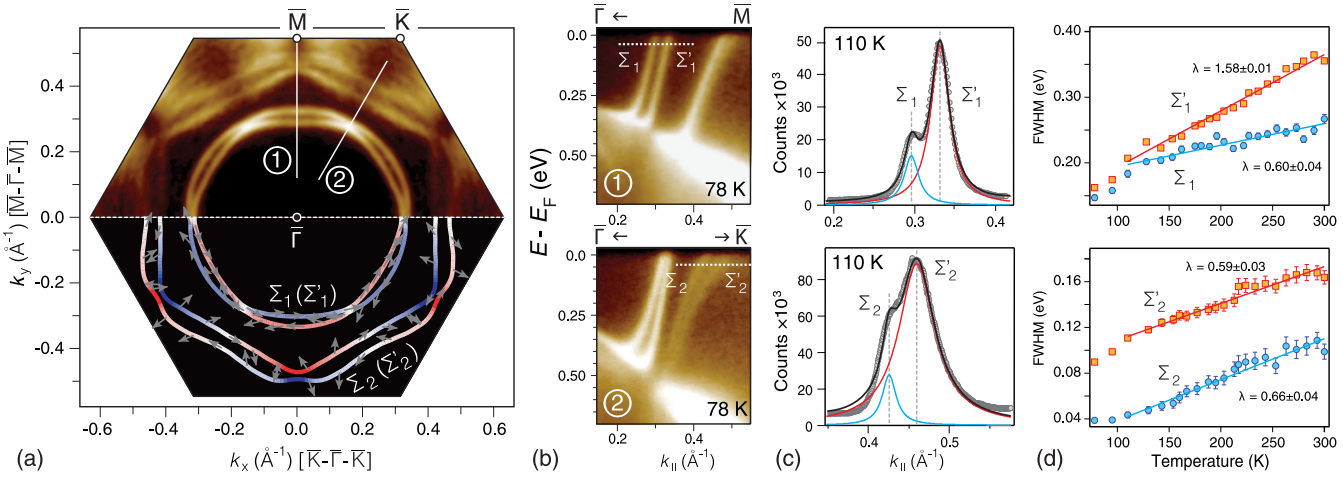

FIG. 2 (color online). (a) Experimental (upper panel) and calculated [12] (lower panel) Fermi contours of the 2D Tl-Pb compound on Si(111) shown in the $\sqrt{3} \times \sqrt{3}$ surface Brillouin zone. Small arrows in the lower panel indicate the in-plane spin components, while the color code indicates the out-of-plane components. (b) Fragments of the ARPES spectra showing dispersion of Σ_1 (Σ_1') and Σ_2 (Σ_2') bands near the Fermi level along $\bar{\Gamma} - \bar{M}$ and $\bar{\Gamma} - \bar{K}$ directions [solid lines 1 and 2 in (a)]. (c) Momentum distribution curves measured along the dashed lines shown in (b) and their Lorentzian-function fits with constant background for Σ_1 (Σ_1') and Σ_2 (Σ_2') bands. (d) Typical temperature dependencies of energy width ΔE for Σ_1 (Σ_1') and Σ_2 (Σ_2') surface-state bands.

has almost round shape, while the inner contour is a hexagon with corners pointing in the $\bar{\Gamma}-\bar{K}$ directions in the $\sqrt{3}\times\sqrt{3}$ surface Brillouin zone. The maximal momentum and energy splittings for the Σ_1 (Σ_1') band, $\Delta k_{\|} = 0.038$ Å^{-1} and $\Delta E_F = 250$ meV, respectively, are along the $\bar{\Gamma}-\bar{M}$ direction. The Σ_2 (Σ_2') bands show up as hexagonal contours with corners along the $\bar{\Gamma}-\bar{M}$ direction. The maximal splittings for the Σ_2 (Σ_2') band, $\Delta k_{\|} = 0.050$ Å^{-1} and $\Delta E_F = 140$ meV, are along the $\bar{\Gamma}-\bar{K}$ direction. DFT calculations revealed that the planar spin components show in-plane helicity with the spin being fully aligned in plane and perpendicular to the momentum vector for momentum vectors along the $\bar{\Gamma}-\bar{K}$ directions. The out-of-plane spin component undulates between positive and negative values along the contours according to the C_{3v} symmetry of the surface.

Superconducting properties are associated with an enhanced electron-phonon scattering whose strength is usually described by the EPC constant λ. In order to determine λ, we used temperature-dependent ARPES data, where λ can be extracted from the slope of the temperature T dependence of the spectral energy width of a surface-state band ΔE according to the relation $\lambda = (d\Delta E/dT)/(2\pi k_B)$, where k_B is the Boltzmann constant. The value of λ at the Fermi level E_F is the most important in electrical conductance [26]. However, dispersion of the Σ_1 and Σ_2 bands is very steep in the vicinity of E_F, which hampers reliable determination of ΔE. Therefore, we first extracted the momentum distribution curves (MDC) and evaluated the width Δk, which is defined as the width of the Lorentzian function fit to the MDC [27] [Fig. 2(c) and also Fig. S1 in Supplemental Material [28]]. The ΔE value was obtained as the product of Δk with the gradient of the dispersion dE/dk near the Fermi level evaluated for each band. Finally, EPC constant λ was determined from a linear fit to the $\Delta E - T$ plots. The temperature range chosen was beyond ~110 K in order to exceed the Debye temperature θ_D, which is known to amount to ~90–100 K for bulk Tl and Pb. For each band, the measurements were conducted in the directions where spin splitting is maximal [i.e., along the $\bar{\Gamma}-\bar{M}$ direction for the Σ_1 (Σ_1') band and along the $\bar{\Gamma}-\bar{K}$ for Σ_2 (Σ_2')] to obtain λ for each subband.

Figure 2(d) shows typical $\Delta E - T$ plots with the results of EPC constant λ evaluation for a particular experimental run. A set of experiments performed with different samples both in heating and cooling regimes yield the following mean values of λ: 0.7 ± 0.1 for Σ_1, 1.6 ± 0.1 for Σ_1', and 0.6 ± 0.05 for both Σ_2 and Σ_2' bands. One can see that the EPC constant λ varies from one band to another and might be different even for two neighboring subbands having opposite spin orientations. However, the difference in the EPC of different bands of the same material is quite a common phenomenon due to the largely varying electron DOS and phonon spectrum for different momentum values [27,30]. It is worth noting also that the relation between the EPC constant and superconducting properties is not straightforward (e.g., λ can be strongly enhanced due to surface and/or interface effects [31]). Nevertheless, the occurrence of the Σ_1' band displaying enhanced EPC provides a promise for observing superconductivity in this (Tl, Pb)/Si(111) system. For comparison, the known superconducting In and Pb monolayers on Si(111) demonstrate lower values of λ, 0.8–1.0 for In [30] and 0.6–0.9 for Pb [32].

The results of the transport measurements on this (Tl, Pb)/Si(111) system at low temperatures are summarized in Figs. 3 and 4. Figure 3(a) shows the temperature dependence of the 2D sheet resistance. One can see that it reaches the zero resistance state around 2.2 K, an evidence of superconductivity. The resistance decreases even above T_c, which is due to the superconducting fluctuation typically observed in 2D superconductors [33]. Accurate fitting of the experimental data with the theory [17,33] yields $T_c = 2.25$ K and also the "pair-breaking parameter" $\delta = 0.12$,

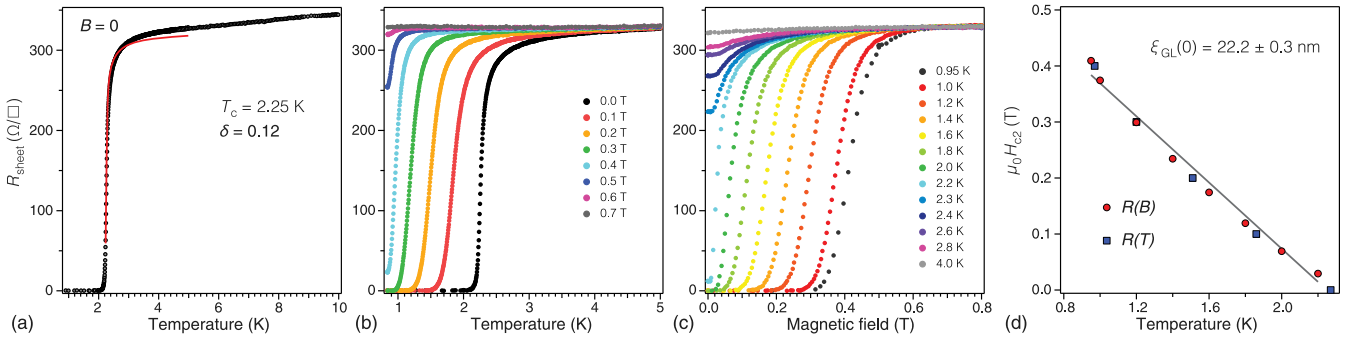

FIG. 3 (color online). (a) Temperature dependence of the sheet resistance. Red line is a result of the least-squares fit to the Aslamazov-Larkin-Maki-Thompson correction [17] with $T_c = 2.25$ K and "pair-breaking parameter" $\delta = 0.12$. The change of the sheet resistance (b) with temperature under different magnetic fields and (c) with magnetic field under different temperatures. (d) Temperature dependence of the upper critical field extracted from temperature (blue squares) and magnetic field (red circles) dependencies of the sheet resistance [from (b) and (c), respectively].

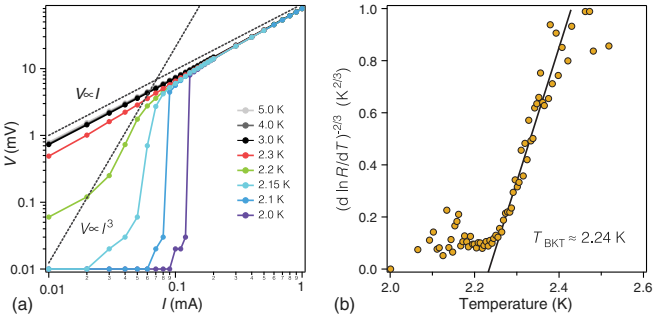

FIG. 4 (color online). (a) $I-V$ characteristics near the critical current around T_c, plotted on a double-logarithmic scale, under zero magnetic field. Two dashed lines indicate $V \propto I$ and $V \propto I^3$ curves. (b) Temperature dependence of $(d \ln R/dT)^{-2/3}$. The solid line depicts the expected BKT transition behavior, to obtain $T_{\mathrm{BKT}} = 2.24$ K.

which is the same order of magnitude as those observed for Nb films [34] and other superconducting surface states on Si [17].

Figure 3(b) shows the sheet resistance as a function of temperature under different magnetic field B applied perpendicular to the surface. The superconductivity transition becomes broader and shifts to lower temperature as B increases. The results of the magnetoresistance measurements at different temperatures are summarized Fig. 3(c). By defining the upper critical field ($H_{c2} = B_{c2}/\mu_0$) at which the sheet resistance is a half of the normal-state resistance in Fig. 3(c), the data are summarized in Fig. 3(d). Evaluation of the obtained data in the framework of the Ginzburg-Landau (GL) theory yields the H_{c2} and GL coherence length $\xi_{\mathrm{GL}}(0)$ at 0 K [17]: $\mu_0 H_{c2}(0) = 0.67 \pm 0.02$ T and $\xi_{\mathrm{GL}}(0) = 22.2 \pm 0.3$ nm. These are on the same order as in the cases of mono- or bilayer superconductors In and Pb on Si(111) [17]. To characterize the type of superconductivity, conventional or unconventional (exotic) [35], one has to compare the GL coherence length with the average distance between Cooper pairs, $s \sim (g_0 \Delta)^{-1/2}$, where g_0 is the 2D density of states at E_F and Δ is the superconducting gap, which is about $2T_c$. Evaluation for the (Tl, Pb)/Si(111) yields that even in the extreme case when all electrons at E_F participate in superconductivity, $s \sim 50$ nm, i.e., $\xi_{\mathrm{GL}}(0) < s$. If only a certain fraction of all electrons are superconducting, the inequality becomes even more strict. This is in contrast to the conventional superconductors for which $\xi_{\mathrm{GL}}(0) \gg s$. Thus, the (Tl, Pb)/Si(111) system shows up plausibly as an unconventional superconductor [35]. In addition, it is worth noting that, in contrast to numerous known superconductors, the Tl-Pb 2D compound as well as other single- and double-atom-layer-thick superconductors do not fit the recently proposed universal scaling relation [29], indicating that they plausibly constitute a very specific type of low-dimensional superconductors (for details, see Sec. S2 of Supplemental Material [28]).

It has been recognized that superconducting transitions in the 2D cases can exhibit signatures of the Berezinskii-Kosterlitz-Thouless mechanism [21,36–38]. For the (Tl, Pb)/Si(111) system, strong support for the BKT transition was found in the current-voltage ($I-V$) isotherms measured over a grid of different temperatures near T_c. Figure 4(a) presents these data plotted in a double-logarithmic scale. Evolution of the isotherms is consistent with a change in exponent of power in $I-V$ curves around the critical current expected from the BKT mechanism when the temperature is varied near T_c. The $I-V$ dependence follows the $V \propto I$ law for the normal state above T_c, while it becomes $V \propto I^3$ around T_c and shows abrupt transition to the superconducting state well below T_c. At the BKT transition, the current-induced Lorentz force causes thermally created vortex-antivortex pairs to unbind, resulting in the $V \propto I^3$ behavior. The extracted BKT transition temperature $T_{\mathrm{BKT}} \sim 2.2$ K. It is also known that the resistance is described by $R \propto \exp\{-b(T/T_{\mathrm{BKT}} - 1)^{-1/2}\}$ near T_{BKT}, with a material-dependent constant b [39]. Figure 4(b) shows that our data are consistent with this behavior and yield $T_{\mathrm{BKT}} = 2.24$ K, in agreement with the result in Fig. 4(a).

In conclusion, the 2D compound of 1 ML Tl with 1/3 ML Pb having $\sqrt{3} \times \sqrt{3}$ periodicity on Si(111) appears to be a 2D material that combines together the giant Rashba-type spin splitting (~250 meV) with the superconductivity at a sizable transition temperature of 2.25 K. This combination provides an opportunity to observe a number of fascinating phenomena. In conventional superconductors the electron pairs are in a spin-singlet state with antiparallel spins. If the space-inversion symmetry is broken and the magnitude of the spin splitting is sufficiently larger than the superconducting gap, the interband Cooper pairing between electrons in the two spin-split bands is strongly suppressed. As a result, the pairing state in one band is the admixture of the spin-singlet and spin-triplet pairing [40], which leads to the advanced properties, some of which have already been considered theoretically [40–45] and experimentally [46]. In particular, it has been predicted that in such systems spin magnetic susceptibility becomes anisotropic and Knight shift retains a finite and rather high value at $T = 0$ [40]. Furthermore, an in-plane magnetic field applied to the 2D superconductor with sizable spin-orbit coupling would induce an in-plane superconducting flow [41]. Strong spin-orbit interaction is expected to broaden the range of existence of the Larkin-Ovchinnikov-Fulde-Ferrell phase, which would take the form of periodic stripes running along the field direction on the surface, leading to the anisotropy of its properties [42,43]. In addition, triplet supercurrents can carry a net spin component and so offer the potential to the superconducting spintronics [22,45].

The ARPES and STM works were supported by the Russian Science Foundation under Grant No. 14-12-00479.

Transport measurements were supported by the Grants-in-Aid for Scientific Research Program from the Japan Society for the Promotion of Science. Encouraging discussions with E. I. Rashba and L. P. Gor'kov are gratefully acknowledged.

*saranin@iacp.dvo.ru

[1] J. J. Lander, Surf. Sci. **1**, 125 (1964).
[2] E. I. Rashba, Sov. Phys. Solid State **2**, 1109 (1960).
[3] Y. A. Bychkov and E. I. Rashba, JETP Lett. **39**, 78 (1984).
[4] I. Gierz, T. Suzuki, E. Frantzeskakis, S. Pons, S. Ostanin, A. Ernst, J. Henk, M. Grioni, K. Kern, and C. R. Ast, Phys. Rev. Lett. **103**, 046803 (2009).
[5] K. Sakamoto, H. Kakuta, K. Sugawara, K. Miyamoto, A. Kimura, T. Kuzumaki, N. Ueno, E. Annese, J. Fujii, A. Kodama *et al.*, Phys. Rev. Lett. **103**, 156801 (2009).
[6] E. Frantzeskakis, S. Pons, and M. Grioni, Phys. Rev. B **82**, 085440 (2010).
[7] K. Sakamoto, T. Oda, A. Kimura, K. Miyamoto, M. Tsujikawa, A. Imai, N. Ueno, H. Namatame, M. Taniguchi, P. E. J. Eriksson *et al.*, Phys. Rev. Lett. **102**, 096805 (2009).
[8] J. Ibañez-Azpiroz, A. Eiguren, and A. Bergara, Phys. Rev. B **84**, 125435 (2011).
[9] K. Sakamoto, T. H. Kim, T. Kuzumaki, B. Müller, Y. Yamamoto, M. Ohtaka, J. R. Osiecki, K. Miyamoto, Y. Takeici, A. Harasawa *et al.*, Nat. Commun. **4**, 2073 (2013).
[10] S. D. Stolwijk, A. B. Schmidt, M. Donath, K. Sakamoto, and P. Krüger, Phys. Rev. Lett. **111**, 176402 (2013).
[11] S. D. Stolwijk, K. Sakamoto, A. B. Schmidt, P. Krüger, and M. Donath, Phys. Rev. B **90**, 161109 (2014).
[12] D. V. Gruznev, L. V. Bondarenko, A. V. Matetskiy, A. A. Yakovlev, A. Y. Tupchaya, S. V. Eremeev, E. V. Chulkov, J. P. Chou, C. M. Wei, M. Y. Lai *et al.*, Sci. Rep. **4**, 4742 (2014).
[13] D. V. Gruznev, L. V. Bondarenko, A. V. Matetskiy, A. Y. Tupchaya, A. A. Alekseev, C. R. Hsing, C. M. Wei, S. V. Eremeev, A. V. Zotov, and A. A. Saranin, Phys. Rev. B **91**, 035421 (2015).
[14] T. Zhang, P. Cheng, W. J. Li, Y. J. Sun, G. Wang, X. G. Zhu, K. He, L. Wang, X. Ma, X. Chen *et al.*, Nat. Phys. **6**, 104 (2010).
[15] S. Qin, J. Kim, Q. Niu, and C. K. Shih, Science **324**, 1314 (2009).
[16] T. Uchihashi, P. Mishra, M. Aono, and T. Nakayama, Phys. Rev. Lett. **107**, 207001 (2011).
[17] M. Yamada, T. Hirahara, and S. Hasegawa, Phys. Rev. Lett. **110**, 237001 (2013).
[18] T. Uchihashi, P. Mishra, and T. Nakayama, Nanoscale Res. Lett. **8**, 167 (2013).
[19] S. Yoshizawa, H. Kim, T. Kawakami, Y. Nagai, T. Nakayama, X. Hu, Y. Hasegawa, and T. Uchihashi, Phys. Rev. Lett. **113**, 247004 (2014).
[20] J. Noffsinger and M. L. Cohen, Solid State Commun. **151**, 421 (2011).
[21] W. Zhao, Q. Wang, M. Liu, W. Zhang, Y. Wang, M. Chen, Y. Guo, K. He, X. Chen, Y. Wang *et al.*, Solid State Commun. **165**, 59 (2013).
[22] C. Brun, T. Cren, V. Cherkez, F. Debontridder, S. Pons, D. Fokin, M. C. Tringides, S. Bozhko, L. B. Ioffe, B. L. Altshuler *et al.*, Nat. Phys. **10**, 444 (2014).
[23] J. W. Park and M. H. Kang, Phys. Rev. Lett. **109**, 166102 (2012).
[24] S. Yoshizawa and T. Uchihashi, J. Phys. Soc. Jpn. **83**, 065001 (2014).
[25] M. Yamada, T. Hirahara, R. Hobara, S. Hasegawa, H. Mizuno, Y. Miyatake, and T. Nagamura, e-J. Surf. Sci. Nanotechnol. **10**, 400 (2012).
[26] I. Matsuda, C. Liu, T. Hirahara, M. Ueno, T. Tanikawa, T. Kanagawa, R. Hobara, S. Yamazaki, S. Hasegawa, and K. Kobayashi, Phys. Rev. Lett. **99**, 146805 (2007).
[27] S. Hatta, T. Noma, H. Okuyama, and T. Aruga, Phys. Rev. B **90**, 245407 (2014).
[28] See Supplemental Material at http://link.aps.org/supplemental/10.1103/PhysRevLett.115.147003, which includes Refs. [16,17,21,24,29], for details of EPC constant determination and evaluation of critical temperature of two-dimensional superconductors in the framework of the recently proposed universal scaling relation.
[29] Y. Ivry, C. S. Kim, A. E. Dane, D. De Fazio, A. N. McCaughan, K. A. Sunter, Q. Zhao, and K. K. Berggren, Phys. Rev. B **90**, 214515 (2014).
[30] S. H. Uhm and H. W. Yeom, Phys. Rev. B **86**, 245408 (2012).
[31] D.-A. Luh, T. Miller, J. J. Paggel, and T.-C. Chiang, Phys. Rev. Lett. **88**, 256802 (2002).
[32] M. Ligges, M. Sandhofer, I. Sklyadneva, R. Heid, K. P. Bohnen, S. Freutel, L. Retting, P. Zhou, P. M. Echenique, E. V. Chulkov *et al.*, J. Phys. Condens. Matter **26**, 352001 (2014).
[33] A. Larkin and A. Varlamov, *Theory of Fluctuations in Superconductors* (Oxford University Press, New York, 2005).
[34] J. W. P. Hsu and A. Kapitulnik, Phys. Rev. B **45**, 4819 (1992).
[35] V. F. Gantmakher and V. T. Dolgopolov, Phys. Usp. **53**, 1 (2010).
[36] V. L. Berezinskii, Zh. Eksp. Teor. Fiz. **59**, 907 (1970) [Sov. Phys. JETP **32**, 493 (1971)].
[37] J. M. Kosterlitz and D. J. Thouless, J. Phys. C **6**, 1181 (1973).
[38] H. M. Zhang, Y. Sun, W. Li, J. P. Peng, C. L. Song, Y. Xing, Q. Zhang, J. Guan, Y. Zhao, S. Ji *et al.*, Phys. Rev. Lett. **114**, 107003 (2015).
[39] B. I. Halperin and D. R. Nelson, J. Low Temp. Phys. **36**, 599 (1979).
[40] L. P. Gor'kov and E. I. Rashba, Phys. Rev. Lett. **87**, 037004 (2001).
[41] S. K. Yip, Phys. Rev. B **65**, 144508 (2002).
[42] V. Barzykin and L. P. Gor'kov, Phys. Rev. Lett. **89**, 227002 (2002).
[43] K. Michaeli, A. C. Potter, and P. A. Lee, Phys. Rev. Lett. **108**, 117003 (2012).
[44] J. P. A. Devreese, J. Tempere, and C. A. R. Sá de Melo, Phys. Rev. Lett. **113**, 165304 (2014).
[45] J. Linder and J. W. A. Robinson, Nat. Phys. **11**, 307 (2015).
[46] T. Sekihara, R. Masutomi, and T. Okamoto, Phys. Rev. Lett. **111**, 057005 (2013).

Supplemental Material for "Two-dimensional superconductor with giant Rashba effect: One-atomic-layer Tl-Pb compound on Si(111)"

A.V. Matetskiy, S. Ichinokura, L.V. Bondarenko, A.Y. Tupchaya, D.V. Gruznev, A.V. Zotov, A.A. Saranin, R. Hobara, A. Takayama, and S. Hasegawa

S1. Temperature-dependent momentum distribution curves for the Σ_1 (Σ'_1) and Σ_2 (Σ'_2) bands

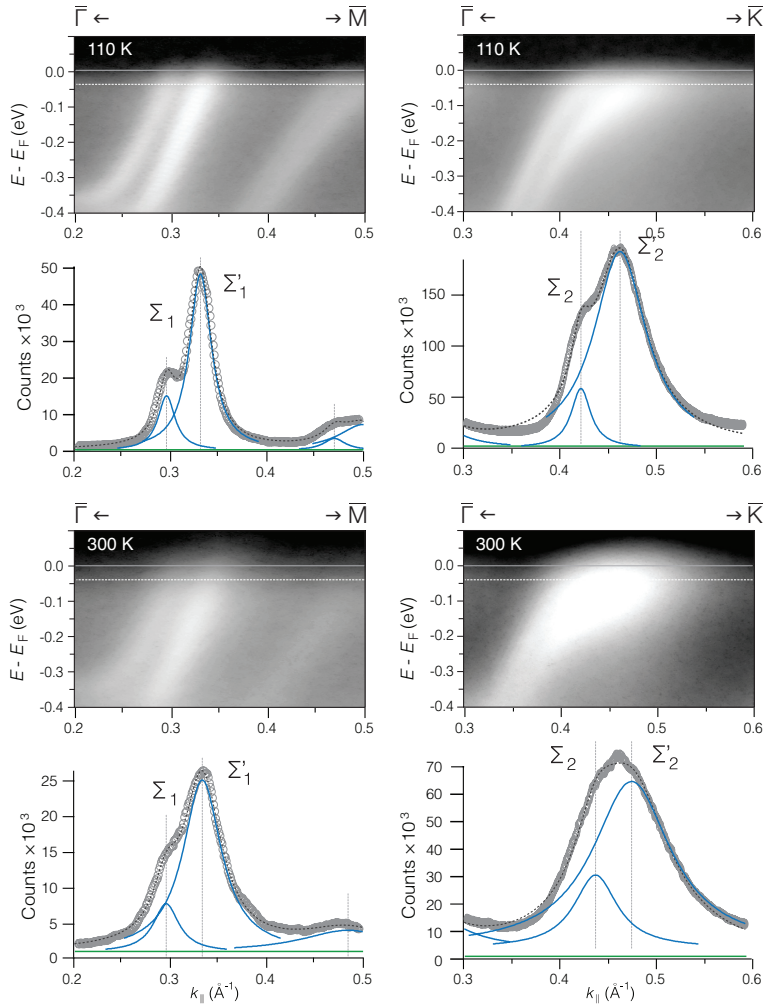

Figure S1: Momentum distribution curves for the Σ_1 (Σ'_1) band (left panel) and the Σ_2 (Σ'_2) band (right panel) extracted from the measured ARPES intensities along the dashed line shown in the spectra. The upper panels show the data acquired at 110 K, the lower panels those acquired at 300 K. The peaks in the MDCs, especially Σ'_1, are clearly shown to be broadened at higher temperature.

S2. Atomic-layer superconductors and universal scaling of the critical temperature

Very recently, Ivry et al. [1] have proposed an universal scaling to tie together the superconducting critical temperature T_c, film thickness d and sheet resistance in the normal metallic state R_s in the form of the relationship

$$d \cdot T_c = A R_s^{-B},$$

where A and B are fitting parameters. It has been demonstrated that numerous various superconducting materials follow the scaling relation (symbols and solid black line in Fig. S2) with molybdenum being the only material outside the trend.

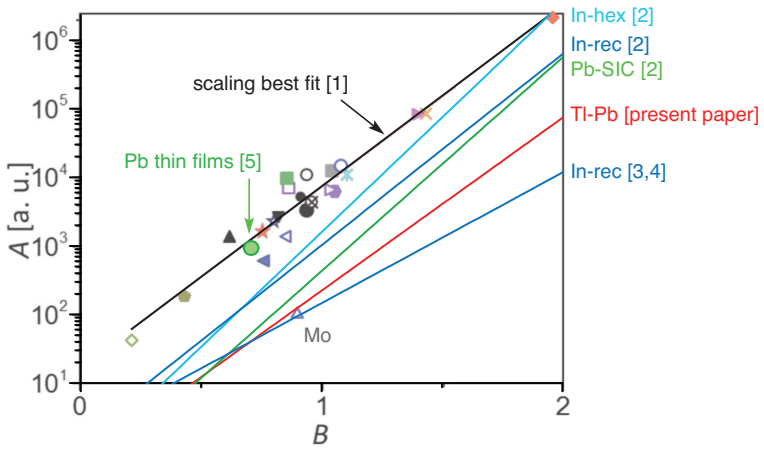

Figure S2: Results of the scaling evaluation for the Si(111)$\sqrt{3}\times\sqrt{3}$-(Tl, Pb) (red line), Si(111)-hex-$\sqrt{7}\times\sqrt{3}$-In (light blue line), Si(111)-rec-$\sqrt{7}\times\sqrt{3}$-In (dark blue line) and Si(111)-SIC-$\sqrt{3}\times\sqrt{3}$-Pb (green line) superposed on the plot of scaling relation (black line) from Fig. S17.1 in Ref. [1]. Green circle denotes the result of evaluation for the Pb thin films [5].

Table S1: Parameters used for evaluation of the scaling relation for the single- and double-atomic-layer-thick films of Tl-Pb, In and Pb and thin Pb films with the thickness ranging from four to eight monolayers

Structure	R_s (Ohm/□)	T_c (K)	d (nm)	note	Ref.
Pb-Tl	330	2.25	0.3	single layer	Present work
SIC-Pb	1300	1.1	0.3	single layer	[2]
hex-In	2200	2.4	0.3	single layer	[2]
rec-In	610	2.8	0.6	double layer	[2]
rec-In	80	3.05	0.6	double layer	[3,4]
Pb	2700	2.5	1.16	thin films	[5]
	1900	3	1.45		
	1100	4.2	1.74		
	700	4.8	2.03		
	300	6	2.32		

We tested if the present (Tl, Pb)/Si(111) system and other known single- and double-atomic-layer-thick superconductors, Si(111)-hex-$\sqrt{7}\times\sqrt{3}$-In [2], Si(111)-rec-$\sqrt{7}\times\sqrt{3}$-In [2, 3, 4] and Si(111)-SIC-$\sqrt{3}\times\sqrt{3}$-Pb [2] fit the scaling relation. Parameters used in evaluation are summarized in the Table, while Figure S2 shows the obtained results superposed on the scaling plot taken from Fig. S17.1 in Ref. [1]. To obtain a point in B-A coordinates, one has to know R_s versus d dependence. For the above reconstructions, one has a single thickness value for each one. We estimated it as ∼0.3 and ∼0.6 nm for single-layer and double-layer reconstructions, respectively. As a result, evaluation for these systems yields lines in the

plot. One can see that all these lines lie aside the universal scaling relation dependence. Thus, one can conclude that these extremely thin superconducting films constitute a principally new specific type of low-dimensional superconductors.

In addition, we evaluated the data presented in Ref. [5] for the four-to-eight ML thick Pb films grown on Si(111) at 100 K. The result of evaluation is shown by the green circle in Fig. S2. One can see that it fits well the scaling relation dependence. Thus, thin films starts to behave in a usual way already at thickness above four monolayers, hence the new type of low-dimensional superconducters is plausibly limited exclusively by the single- and double-atomic layers only.

References

[1] Y. Ivry, C. S. Kim, A. E. Dane, F. De Fazio, A. N. McCaughan, K. A. Sunter, Q. Zhao, K. K. Berggren, Universal scaling of the critical temperature for thin films near the superconducting-to-insulating transition, Phys. Rev. B 90 (2014) 214515.

[2] M. Yamada, T. Hirahara, S. Hasegawa, Magnetoresistance measurements of a superconducting surface state of In-induced and Pb-induced structures on Si(111), Phys. Rev. Lett. 110 (2013) 237001.

[3] T. Uchihashi, P. Mishra, M. Aono, T. Nakayama, Macroscopic superconducting current through a silicon surface reconstruction with indium adatoms: Si(111)-($\sqrt{7}\times\sqrt{3}$)-In, Phys. Rev. Lett. 107 (2011) 207001.

[4] S. Yoshizawa, T. Uchihashi, Superconducting phase transition of the Si(111)-($\sqrt{7}\times\sqrt{3}$)-In surface: Solution of T_c discrepancy, J. Phys. Soc. Japan. 83 (2014) 065001.

[5] W. Zhao, Q. Wang, M. Liu, W. Zhang, Y. Wang, M. Chen, Y. Guo, K. He, X. Chen, Y. Wang, J. Wang, X. Xie, Q. Niu, L. Wang, X. Ma, J. K. Jain, M.H.W. Chan, Q.-K. Xue, Evidence for Berezinskii-Kosterlitz-Touless transition in atomically flat two-dimensional Pb superconducting films, Sol. State Commun. 165 (2013) 59.